The impact of mir200 on extracellular matrix topography–guided epithelial–to–mesenchymal transition of prostate cancer cells

Tuğba Özdemir

ABSTRACT

Objective: Epithelial to Mesenchymal Transition (EMT) is an important phenomenon that is recently been recognized to play roles on prostate cancer metastasis through both epigenetic and biochemical signaling pathways. Using tissue engineering tools, we recreated a metastatic tumor niche to study the role of mir200 (a small RNA proven to reverse EMT processes) on extracellular matrix (ECM) fiber diameter guided prostate cancer cell EMT.

Material and methods: LNCaP cells were cultured on fibrous scaffolds for 48 hours. Role of fiber diameter (0.5 and 5 μm respectively) on cell morphology, viability, metabolic rate and EMT characteristics was assessed. Finally, the cells on fibers were transfected with a mir200 precursor to study the synergy between substrate topography and epigenetic signals on EMT of LNCaP prostate cancer cells.

Results: LNCaP cells formed cell clusters on fibers with 0.5 μm diameter while they form spindle shaped single cells possessing mesenchymal-like morphology when they were cultured on 5 μm diameter polymer fibers. The metabolic rate of cells growing on 5 μm fibers showed a substantial increase at 48 hours compared to flat topography or 0.5 μm- diameter fiber topography. LNCaP morphology is significantly different. Epithelial markers were stained positive on cells growing on small fibers while mesenchymal markers were positive on cells growing on large diameter fibers. mir200 did not alter the observed cell morphology on large diameter fibers.

Conclusion: Our results indicate that substrate topography is the governing signal for LNCaP prostate cancer cells to undergo EMT and mir200 did not reverse the EMT morphology on large diameter fibers.

Keywords: Electrospinning; epithelial-to-mesencymal trasition; LNCaP cells; mir200; PCL

ORCID IDs of the authors:
T.Ö. 0000–0002–0291–5293.

Department of Genetics and Bioengineering, Gaziosmanpaşa University Faculty of Engineering, Tokat, Turkey

Correspondence:
Tuğba Özdemir
E–mail:
tugbaozdemir.tr@gmail.com

Introduction

Prostate cancer microenvironment consists of heterogenous population of cancer cells with epithelial characteristics and cancer cells with mesenchymal characteristics.[1] Recent studies indicate that this epithelial to mesenchymal heterogeneity is the underlying cause of metastatic tumor extravasation.[2] The cellular physiological phenomenon called epithelial to mesenchymal transition (EMT) is a process where cells with epithelial characteristics (cobble stone morphology, tight cell-cell junctions and low migration tendency) undergo a series of morphological and transcriptional transformations that lead to the development of cells with mesenchymal characteristics (spindle shape morphology, absent cell-cell junctions and high migratory capacity).[3] Accumulating evidence shows that EMT plays roles in prostate cancer transmigration from the initial tumor site and distant metastatic colony progression.[4]

In addition to a heterogenous cell population, prostate cancer microenvironment undergoes a series of changes within the extracellular matrix (ECM).[5] One of the hallmarks of prostate

cancer progression is the increased ECM collagen fiber diameter. Invasive cells use the newly formed fibrils as highways to escape the primary tumor site and intravasate to enter blood stream in order to spread to other organs.[1] Although the mechanism by which the cells increase their ECM production has not been proven yet, it is important to understand why and how cells utilize the newly formed ECM and also undergo EMT.[6-9] This makes it important to understand the role of the fiber diameter in tumor progression and their crosstalk with EMT.

Epithelial to mesenchymal transition is a reversible process which is regulated through genetic or epigenetic pathways. Based on the microenvironmental conditions EMT cells can reverse their state and undergo mesenchymal to epithelial transition (MET).[10] It is recently proven that microRNA molecules play important roles in this plastic cell state. One of the most important microRNAs that were proven to reverse EMT is mir200.[11,12] mir200 can re-establish epithelial markers via downregulating transcription factor ZEB-1. Decrease in ZEB-1 results in an increase in E-Cadherin which is an epithelial cell marker.[13,14] However earlier studies on mir200 were perfomed using 2D surfaces which are not realistic representations of prostate cancer ECM.

Biomaterials can be used to create realistic *in vitro* structures that truly represent the architecture of prostate cancer ECM such as collagen-like fibers. One of the techniques to create synthetic fibers is electrospinning.[7] Electrospinning is a process to create ECM mimetic fibers by drawing a polymer solution from a syringe, and placing them onto a conductive substrate. Using electrospinning technique polymeric fibers with controlled diameter can be reproduced which are structurally identical to the collagen fibers in prostate cancer ECM.[15]

In this study, we developed an *in vitro* cancer model by creating two different fiber structures reminiscent of healthy and metastatic prostate microenvironment. The synthetic fiber structures were built to understand the effect of ECM fiber diameter on EMT behavior of LNCaP prostate carcinoma cell line. We further tested a small RNA known to reverse EMT on variety of epithelial cells and investigated the synergy between surface topography and epigenetic cues. Our results shed light onto the clarification of the mechanism of metastatic progression from an engineering standpoint.

Material and methods

Chemicals and reagents
Poly (ε-caprolactone) (PCL, ~ 80 kDa) (Sigma-Aldrich, St. Louis, MO, USA), dichloromethane (DCM) (Sigma-Aldrich, St. Louis, MO, USA), isopropanol (IPA) (Sigma-Aldrich, St. Louis, MO, USA), chloroform (Sigma-Aldrich, St. Louis, MO, USA), *N,N*-dimthylformamide (DMF) (Sigma-Aldrich, St. Louis, MO, USA),

hexamethylenediamine (HMD) (Sigma-Aldrich, St. Louis, MO, USA), di-functional cross-linker sulfosuccinimydyl 4-(*N*-maleimidomethyl) cyclohexane-1-carboxylate (sulfo-SMCC) (Thermo-Fisher, Rockford, IL, USA), Penicillin/Streptomycin (Thermo-Fisher, Rockford, IL, USA). RPMI Media and Fetal Bovine Serum (ATCC, Manassas, VA, USA). Anti-mouse ZEB-1 monoclonal antibody Santa Cruz Biologicals, Dallas, TX, USA) and purified mouse anti-E Cadherin antibody (BD Biosciences, Franklin States, NJ, USA). Alexa488-conjugated goat anti mouse secondary antibody and Alexa568-conjugated Phalloidin dye, DAPI, Syto 13, Propidium Iodide, Presto Blue and transfection reagents targeting mir200 (Thermo-Fisher Scientific Eugene, OR, USA).

Fabrication of fibrous scaffolds and flat polymer topography
Fibers with different diameters were fabricated using our previously established protocol of electrospinning.[15] Briefly, PCL polymer solution was prepared and loaded into a syringe pump. For 5 μm diameter fibers 15% PCL dissolved in chloroform, and for 0.5 μm fibers 12% PCL dissolved in 7:3 DCM:DMF were used. An electric field was generated between the polymer extruding syringe needle and a conductive collector. The fibers with desired diameter were collected onto the conductive surface until the mat reached approximately 130 μm thickness and the mats were further dried in a vacuum chamber to discard the remaining solvents. The PCL fiber mats were further conjugated with RGD (Arginine-Glycine and Aspartic acid) using surface amination and further crosslinking in the presence of a difunctional linker (sulfo-SMCC) as detailed before.[15] The RGD functional PCL fiber mats were then sterilized for further cell culture seeding. Flat PCL topographies created by spun were coated onto glass slides by 5% w/v PCL in chloroform solution and further annealed at 60 °C in order to fix onto the glass slides.

Cell culture
LNCaP cells generously provided by Dr. Leland Chung were maintained in RPMI media containing 5% FBS and 1000 IU/mL Penicillin/Streptomycin in a 37^{0}C and 5% CO_2 incubator with a 95% humidity. When the cells reached 80% confluency they were lifted off by using trypsin and neutralizing with culture media. The resuspended cells were further spinned down in a 1500 rpm for 5 mins to get a loose cell pellet. The cells were then diluted into a desired concentration to be seeded onto the sterilized and washed fibrous scaffolds. Each 10 mm disc shaped scaffolds were seeded with 50,000 LNCaP cells and incubated for 48 hours before processing the scaffolds for further biological characterization experiments.

Cell viability experiments
Our attempt was to understand the cell-surface interactions, therefore the experimental period-the time period before the cells proliferated and covered the whole available surface- was kept short (48 hours). After an initial culture period of 48 hours, fibrous scaf-

fold discs with LNCaP cell were transferred from incubator into a clean glass bottom 8 well NUNC-chambers for assessing cell viability characterization. The cells were washed with warm PBS once to remove unbound cells and cell debris on the surface. Next, a mixture of SYTO13 (1:1000) (Thermo-Fisher, Rockford, IL, USA) and propidium iodide (1:2000) (Thermo-Fisher, IL, USA) in warm PBS was added and the scaffolds were incubated for 15 minutes. After 15 mins the scaffolds were washed with warm PBS gently for 3 times and immediately imaged using a ZEISS LSM710 confocal microscope (Carl Zeiss, Maple Grove, MN, USA) at 10x magnification. Three confocal images were obtained for each surface topography including a flat surface spun coated with PCL as control with no surface curvature. In addition to staining the live and dead cells, one more viability assay was conducted to confirm the metabolic activity of the cells that were grown on different surface topographies. The Presto blue reagent (Thermo-Fisher, Rockford, IL, USA) was pipetted into the empty wells containing fibrous discs or glass 10mm-discs coated with flat PCL and incubated 2 hours at 37^0C and 5% CO_2 incubator with a 95% humidity and after the incubation period the fluorescence intensities of the supernatants were read with a Wallac 1420 Victor2 fluorescence plate reader (Perkin Elmer, Rodgau, Germany).

Immunofluorescence staining
LNCaP cells were fixed with ice cold cytoskeleton stabilization buffer (CSB) for 1 min. Then 4% paraformaldehyte (PFA) solution was added onto the scaffolds and incubated for 15 mins. After PFA fixation, the cells were washed thrice for 5 min each, permeabilized and blocked with a PBS solution that contained 2% BSA and 0.1% TX100 (PB Buffer) for 45 mins. After blocking, the cells were then incubated with a primary antibody diluted (ZEB-1 1:50 and ECAD 1:100) in the PB buffer for 90 mins. After 90 mins the scaffolds washed thrice with PBS for 15 min each to wash away unbound antibodies. The secondary antibodies conjugated with Alexafluor dyes were diluted in PB buffer and incubated for 45 mins. Following secondary antibody incubation, scaffolds were washed thrice for 15 min and Phalloidin and DAPI dyes diluted in PB Buffer were added for cytoskeleton and nuclear staining respectively. After the scaffold immunofluorescence labeling was completed the scaffolds were imaged using Zeiss LSM 880 Multiphoton Confocal Microscope (Carl Zeiss, Maple Grove, MN, USA).

mir200 precursor transfection
LNCaP cells were trypsinized, lifted off the surface, neutralized and counted for the experiment. A total of 10^6 cells were transfected with a pe-mir-200b microRNA precursor and a microRNA negative control using siPORT transfection reagent (Thermo-Fisher, Rockford, IL, USA) following the instructor's manual. After the preincubation period the cells were seeded onto the scaffolds at 100,000 cells/scaffold cell density in triplicates. Twenty-four hours after seeding the scaffolds the culture media was replenished very carefully to remove the transfection

reagent. After the experimental time-period, the cell morphology was assessed using phalloidin and DAPI dyes following the immunostaining protocol and imaged using confocal microscope.

Statistical analysis
All measurements were done in triplicate. Statistical significance was determined using Student's t-test. A p value of <0.05 was considered to be statistically significant.

Results

LNCaP cell morphology, viability and metabolic activity on fibers
The metabolic activity and cellular morphology of LNCaP cells on three different topographies were tested to see whether topography has an overall impact on cellular metabolism.

The metabolic activity of the LNCaP cells on all topographies were shown in Figure 1. The metabolic rate measured was directly correlated with metabolic activity. The relative fluorescence intensity of cells grown on flat topography appeared to be the lowest. The cells grown on 0.5 μm had approximately two-fold higher fluorescence intensity than flat topography. The fluorescence intensity of LNCaP cells was the highest on large diameter fibrous scaffolds (5 μm) showing almost four-fold higher fluorescence intensity than the flat topography and two-fold higher fluorescence intensity than LNCaP cells grown on fibrous scaffolds with a diameter of 0.5 μm.

Next, we looked at the cell viability performing Live/Dead assay and using confocal imaging (Figure 2). In this assay, the viable cells appear green and dead cells red. This assay also gives an overall information about cell shape. In all images cells appeared to be viable as all the cells stained with green and almost no red cells were observed. In Figure 2a the cells appear to form clusters and large groups. In Figure 2b similar LNCaP clusters are observed (outlined with red circles). The LNCaP morphology was spindle shaped when they were grown on 5 μm fibrous scaffolds. Almost no clusters were observed. The figure insets for Figure 2b and 2c shows the higher magnification of the cells.

Epithelial-to-mesenchymal transition of LNCaP cells on fibrous scaffolds
During cancer progression diameters of collagen fibers increase drastically. Therefore, we investigated the EMT behavior of LNCaP cells on changing fiber diameter. Synthetic fibers with 5 and 0.5 μm diameters were created and cells were immunostained for an epithelial marker (E-Cadherin, E-CAD) and a mesenchymal marker (zinc finger E-box binding homeobox *1*, ZEB-1). Confocal images confirmed the observed morphology on both fiber topographies, namely LNCaP cells on 0.5 μm fibers were cobble-stone shaped and LNCaP cells on 5 μm fibers were spindle shaped.

Immunostaining followed by confocal imaging was performed on LNCaP cells growing on 0.5 μm and 5 μm- fibrous scaffolds by targeting an epithelial marker (E-Cadherin, E-CAD) and a mesenchymal marker directly linked to mir200 (zinc finger E-box binding homeobox 1, ZEB-1).

Figure 3 shows the E-CAD (green), F-actin (red) and nucleus (blue) of the cells, and merge shows the overlay of all the targets imaged. Figure 3a-d shows the LNCaP cell clusters grown on 0.5 μm-fibrous scaffolds. E-CAD images show the continuous line between the cells rather than a diffuse E-CAD signal throughout the cells. F-actin image also overlaps with E-CAD signal. Cell nucleus appears to be intact without any condensa-

tion. Figure 3e-h shows the cells grown on 5 μm- fibrous scaffold and also confirms the cell morphology identified with Live/Dead imaging. LNCaP cells on 5 μm- fibrous scaffolds appear to be single and spindle shaped extending over the fiber architectures. E-CAD signal is both at the cell cortex as well as diffuse throughout the cell body. F-actin do not overlap with the E-CAD signal, rather it is weaker than the E-CAD signal and concentrated on the points where cells bound to the fibers. Nucleus is also intact on LNCaP cells grown on 5 μm-fibrous scaffolds.

Figure 4 shows the ZEB-1 (magenta), F-actin (cyan) and nucleus (yellow) of the cells, and merge shows the overlay of all the targets imaged. Figure 4a-d shows the images of cells grown on 0.5 μm-

Figure 1. LNCaP prostate cancer cell metabolic rate was measured on different topographies using Presto Blue Assay. Metabolic activity of the LNCaP cells grown on flat surfaces, 0.5 μm and 5 μm fibers. The graph shows the relative fluorescence intensities of Presto Blue reagent after 36 hours of cell seeding onto the substrates
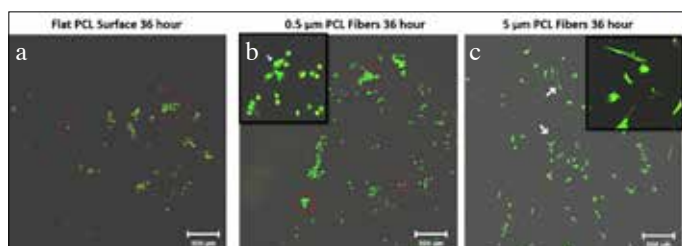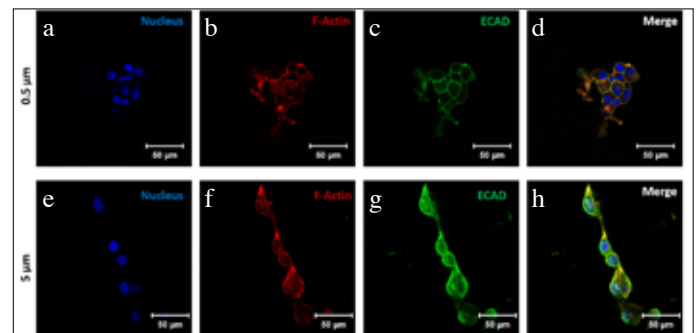*represents statistical significance compared to flat topography $p<0.05$

Figure 2.a-c. LNCaP cellular morphology was examined using confocal fluorescence microscopy on flat topography, 0.5 μm, 5 μm fibers. Green fluorescence represents Syto13 (live cell marker) and red fluorescence represents propidium iodide (dead cell marker). The red circles show the cell clusters on flat and 0.5 μm- fiber topographies. The scale bar is set for 200 μm for all images

Figure 3. a-h. Epithelial characteristics of LNCaP cells growing on flat topography, 0.5 μm, and 5 μm fibers were investigated by immunostaining followed by confocal fluorescence microscopy. Confocal fluorescence images of an epithelial marker protein ECAD for cells grown on 0.5 μm, and 5 μm fibers. Blue represents DAPI staining for nucleus, red , phalloidin staining for actin cytoskeleton, green, ECAD immunostaining for cell-cell junctions and Merge, the overlay of all three images. Scale bar is set for 50 μm
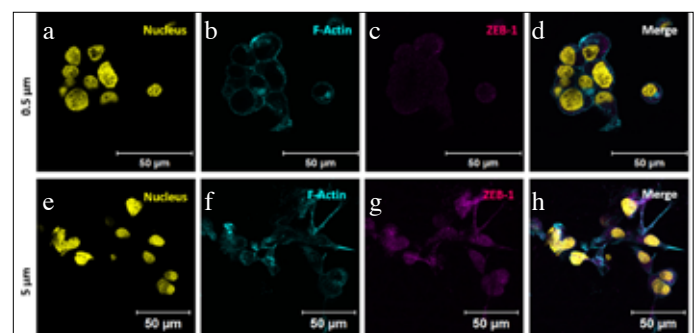

Figure 4.a-h. Mesenchymal characteristics of LNCaP cells growing on flat topography, 0.5 μm, 5 μm fibers were investigated by immunostaining followed by confocal fluorescence microscopy. Yellow represents DAPI staining for nucleus, cyan, phalloidin staining for actin cytoskeleton, magenta, ZEB-1 which is a mesencymal marker and Merge the overlay of all three images. Scale bar is set for 50 μm
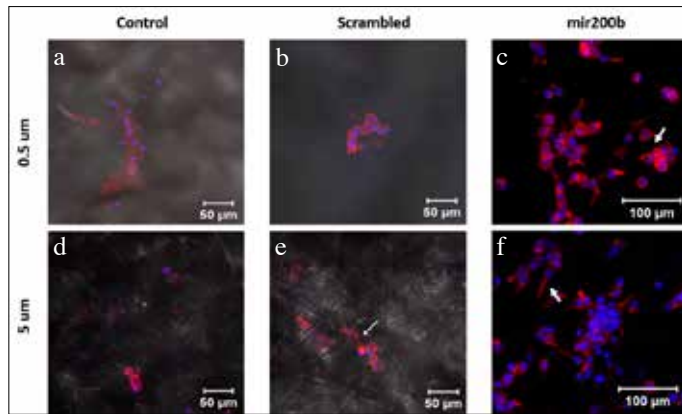
Figure 5.a-f. Cellular cobblestone morphology of LNCaP cells growing on 5 μm and 0.5 μm- fibers after introducing mir200 was examined by confocal fluorescence microscopy. Confocal fluorescence images of LNCaP cell morphology after transfection with mir200 precursor. F-actin (red) is used to define the cell morphology and nucleus (blue) indicates cell locations. Scale bar is set for 50 μm for a-e and 100 μm for c, f
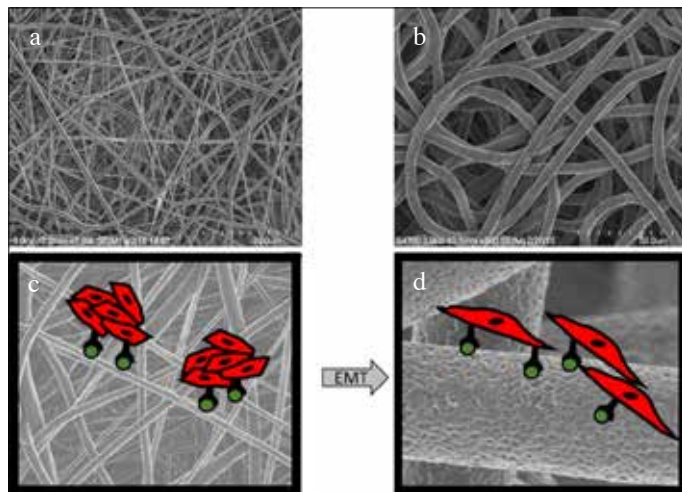

Figure 6. a-d. Schematic representation of the role of fiber diameter on EMT behavior of prostate cancer cells. The SEM images of PCL fibers with 0.5 and 5 μm, respectively

fiber scaffold targeting a mesenchymal marker ZEB-1 (Figure 4c). In Figure 4c almost invisible ZEB-1 signal is present while F-Actin (Figure 4b) still shows the cell boundaries and an intact nucleus (Figure 4a). Conversely Figure 4f shows the intense ZEB-1 signal inside LNCaP cells grown on 5 μm- fiber scaffolds focusing densely inside the nucleus. F-actin signal appears around the cell periphery and it is mainly intense around the points where cells attach the fibers.

Effect of mir200 transfection on fiber topography guided EMT of LNCaP cells

mir200 epigenetic regulator of EMT was shown earlier to reverse EMT of metastatic cancer cells.[11] Therefore we introduced

mir200 into the LNCaP cells cultured on different topographies in order to understand whether the observed EMT behavior on 5 μm- fiber scaffolds could be reversed with mir200. LNCaP cells mir200 precursors, a scrambled sequence and control which only has the transfection reagent were introduced into the cells. Figure 5a-c shows the morphology of LNCaP cells grown on 5 μm- fibrous scaffolds while Figure 5d-f shows the cells on 0.5 μm- fibrous scaffolds. The negative mir transfection shows the effect of transfection reagents on cell morphology and it appears to have no effect on cell morphology. When F-actin (Red) and nucleus (blue) signals between different topographies after mir200 transfection compared, cells were still showing morphological differences that were originated by the substrate topography. White arrows on Figure 5c and Figure 5f show the characteristic morphology was not disrupted by mir200 transfection.

Discussion

Building synthetic tumor models offers a unique opportunity to tune the microenvironmental parameters independently. In this study, we investigated whether a proven epigenetic regulator mir200 influence ECM fiber diameter- guided prostate cancer cell EMT in a realistic *in vitro* tumor model. We showed for the first time in the literature that LNCaP cells undergo EMT phenomenon with an increase in ECM fiber diameter. Further, using our synthetic *in vitro* tumor model we studied the effect of a known EMT regulator shown to reverse EMT on cancer cells.[14,16] We also proved that mir200 cannot reverse EMT on 5 μm-fibrous scaffolds. Figure 6 is a schematic representation of the role of ECM fiber diameter on LNCaP cell behavior.

In earlier studies 3D tumor models were generated using collagen gels and by increasing the concentration of collagen ECM fibers with larger diameters could be generated.[17] However, with increased protein concentration the bioactive ligand concentration would also increase which made it harder to delineate the effect of topography from ligand concentration. Using synthetic polymer fibers, we could be able to depict the role of substrate topography from bioactive ligand concentration.

Utilizing biomaterials and tissue engineering strategies to create disease models is a promising strategy. Physical cues of the ECM are proven to play roles in EMT behavior and provide information about metastatic progression. Saha et al.[7] investigated the role of ECM fiber alignment on breast cancer EMT and further metastatic invasion using PCL fibers and showed that breast cancer cells increased their TGF-Beta 1 levels on aligned fibers as opposed to flat topographies. Similarly, Ravikrishnan et al.[15] created an RGD functionalized fiber topography and investigated the role of fiber diameter on kidney epithelial cell (MDCK) EMT. They showed that the large diameter fibers foster MDCK cell EMT whereas small diameters promote epithelial cell cluster formation and preservation of epithelial morphology of MDCK cells.

Although, there is strong evidence of the relationship between metastatic progression and EMT for many cancer types, the relationship between prostate cancer and EMT is recently being under investigation. In their 2017 paper, Montanari et al.[1] reviewed the recent literature on the relationship between EMT and prostate cancer. They pointed out that LNCaP cells can undergo EMT via androgen receptor driven mechanisms and the mir200 family RNAs have the capacity to reverse this process. The literature existing on prostate cancer metastasis doesn't have enough information on the triad of EMT, ECM cues and prostate cancer metastasis.[16] In our study, we showed that LNCaP prostate cancer cell EMT phenotype is governed by increased ECM fiber diameter. This topography-guided EMT cannot be reversed with mir200. On the other hand, our synthetic fibers did not degrade during the time we performed our experiments. However, during EMT-MET conversion, cells secrete matrix metalloproteases (MMP) to degrade the thick collagen fibers. Future studies will investigate MMP degradable fibers and potential reversal of EMT with mir200.

References

1. Montanari M, Rossetti S, Cavaliere C, D'Aniello C, Malzone MG, Vanacore D, et al. Epithelial-mesenchymal transition in prostate cancer: an overview. Oncotarget 2017;8:35376-89. [CrossRef]

2. Friedl P, Alexander S. Cancer invasion and the microenvironment: plasticity and reciprocity. Cell 2011;147:992-1009. [CrossRef]

3. Kalluri R, Weinberg RA. The basics of epithelial-mesenchymal transition. J Clin Invest 2009;119:1420-8. [CrossRef]

4. Schindeler A, Kolind M, Little DG. Cellular transitions and tissue engineering. Cell Reprogram 2013;15:101-6.

5. Nelson CM, Bissell MJ. Of extracellular matrix, scaffolds, and signaling: tissue architecture regulates development, homeostasis, and cancer. Annu Rev Cell Dev Biol 2006;22:287-309. [CrossRef]

6. Scanlon CS, Van Tubergen EA, Inglehart RC, D'Silva NJ. Biomarkers of epithelial-mesenchymal transition in squamous cell carcinoma. J Dent Res 2013;92:114-21. [CrossRef]

7. Saha S, Duan X, Wu L, Lo PK, Chen H, Wang Q. Electrospun fibrous scaffolds promote breast cancer cell alignment and epithelial-mesenchymal transition. Langmuir 2012;28:2028-34. [CrossRef]

8. Rastaldi MP, Ferrario F, Giardino L, Dell'Antonio G, Grillo C, Grillo P, et al. Epithelial-mesenchymal transition of tubular epithelial cells in human renal biopsies. Kidney Int 2002;62:137-46. [CrossRef]

9. O'Connor JW, Gomez EW. Biomechanics of TGFbeta-induced epithelial-mesenchymal transition: implications for fibrosis and cancer. Clin Transl Med 2014;3:23. [CrossRef]

10. Huang S, Susztak K. Epithelial Plasticity versus EMT in Kidney Fibrosis. Trends Mol Med 2016;22:4-6. [CrossRef]

11. Abba ML, Patil N, Leupold JH, Allgayer H. MicroRNA Regulation of Epithelial to Mesenchymal Transition. J Clin Med 2016;5:pii: E8. [CrossRef]

12. Hilmarsdottir B, Briem E, Bergthorsson JT, Magnusson MK, Gudjonsson T. Functional Role of the microRNA-200 Family in Breast Morphogenesis and Neoplasia. Genes (Basel) 2014;5:804-20. [CrossRef]

13. Bracken CP, Gregory PA, Kolesnikoff N, Bert AG, Wang J, Shannon MF, et al. A double-negative feedback loop between ZEB1-SIP1 and the microRNA-200 family regulates epithelial-mesenchymal transition. Cancer Res 2008;68:7846-54. [CrossRef]

14. Brabletz S, Brabletz T. The ZEB/miR-200 feedback loop--a motor of cellular plasticity in development and cancer? EMBO Rep 2010;11:670-7. [CrossRef]

15. Ravikrishnan A, Ozdemir T, Bah M, Baskerville KA, Shah SI, Rajasekaran AK, et al. Regulation of Epithelial-to-Mesenchymal Transition Using Biomimetic Fibrous Scaffolds. ACS Appl Mater Interfaces 2016;8:17915-26. [CrossRef]

16. Khan MI, Hamid A, Adhami VM, Lall RK, Mukhtar H. Role of epithelial mesenchymal transition in prostate tumorigenesis. Curr Pharm Des 2015;21:1240-8. [CrossRef]

17. Griffith LG, Swartz MA. Capturing complex 3D tissue physiology in vitro. Nat Rev Mol Cell Biol 2006;7:211-24. [CrossRef]